Fluid Flow and Thermodynamic Analysis of a Wing Anti-Icing System

Jun Hua * Hugh H.T. Liu *

ABSTRACT

In this paper, a Navier-Stokes analysis is presented for a thermal aircraft wing anti-icing system. A three-dimensional (3-D) wing leading edge bay model and its two-dimensional (2-D) bay-slice approximation models are simulated using computational fluid dynamics (CFD). The numerical results and their comparative study address the 2-D approximation for the benefit of computational efficiency. Furthermore, the bay skin temperature distributions are obtained by an integrated interior–exterior thermodynamic analysis. It takes into account the skin heat transfer and conductivity. The 2-D CFD results may overestimate the heat transfer, but the surface temperature near the wing leading edge is within the flight test data range.

RÉSUMÉ

Dans le présent document, une analyse Navier-Stokes est présentée pour un système antigivrage thermique de voilure d'aéronef. Un modèle de bord d'attaque de voilure en trois dimensions (3D) et des modèles d'approximation de profil en deux dimensions (2D) sont simulés au moyen de la simulation numérique de la dynamique de fluides (CFD). Les résultats numériques et leur étude comparative traitent de l'approximation en deux dimensions pour le bénéfice de l'efficacité numérique. De plus, la distribution des températures sur le revêtement est obtenue par une analyse thermodynamique intégrée intérieur-extérieur. Elle prend en compte le transfert de chaleur au revêtement et la conductibilité. Les résultats CFD à deux dimensions peuvent surestimer le transfert de chaleur, mais la température superficielle près du bord d'attaque de la voilure s'inscrit dans la plage des données d'essai en vol.

* Institute for Aerospace Studies
University of Toronto
4925 Dufferin Street
Toronto, ON M3H 5T6, Canada
E-mail: liu@utias.utoronto.ca

Received 26 August 2003.

1. INTRODUCTION

The thermal anti-icing system is installed on most passenger airplanes. It introduces hot bleeding air from the power plant into the wing leading edge, to keep the skin surface temperature above the icing condition. The wing surface temperature is controlled through regulating the hot flow passing a wing anti-icing valve by an automatic control system. Recently, the University of Toronto Institute for Aerospace Studies (UTIAS) initiated a research project in this area for the wing anti-icing control system development and analysis. At the initial stage, our investigation focuses on the skin temperature prediction model development. In this paper, we present our research work of the model analysis using the CFD methods and tools.

Compared with conventional analytical methods (Frick and McCullough, 1942), the most recent anti-icing research efforts have focused on using the CFD technique (Bourgault et al., 2000; Beaugendre et al., 2003; Morency et al., 1999; de Mattos and Oliveira, 2000; Wang et al., 2003) and have demonstrated its strong potential. The main purpose of this paper is to apply the existing CFD tools to assist the system modeling and simulation analysis, especially the skin temperature distributions. Therefore, the CFD analysis presented in this paper mainly consists of two steps:

(1) A 2-D bay-slice thermal model is proposed to represent the 3-D physical bay of the wing section, for the benefit of computational efficiency. To evaluate the 2-D slice approximation, this paper presents the investigation of fluid analysis for both a 3-D bay model and its 2-D slice approximation model, as well as the comparison of the detailed flow fields inside a 3-D wing leading edge bay with that of the corresponding 2-D slice bay sections.

(2) To predict the bay skin temperature distributions more accurately, this paper further provides thermal flow characteristics and temperature values both inside and outside the leading edge bay. Skin conditions with heat transfer and conductivity are taken into account in an integrated interior–exterior thermodynamic analysis. As a result, the wing leading-edge skin temperature distributions are presented in responding to certain flight conditions and the hot air inlet configurations.

The remaining part of this paper is organized as follows. In Sect. 2, the 3-D bay model and its 2-D slice approximation

models are simulated. Their numerical results are compared and evaluated. In Sect. 3, the integrated interior–exterior thermal and flow analysis is presented. Finally, the concluding remarks are offered in Sect. 4.

2. Flow Field Analysis for a Bay Model

2.1. The Three-Dimensional Bay Model

The thermal anti-icing system introduces the hot bleeding air into a piccolo tube inside the leading edge of the wing. The hot air then injects from the small holes on the piccolo tube and impinges the inner surface of the leading edge skin to heat it. The outer surface of the skin is then kept at a certain temperature high enough for anti-icing or de-icing operations. Along the wingspan inside the leading edge, there are normally a number of ribs to configure the contours of the skin and to support the piccolo tube. These ribs then form a number of span-wise segments; these are called bays. The hot air inside the bays exits either from exhaust hoses or through certain exhaust collection systems. The most important characteristics to us are the surface temperature distributions. The flow structure inside the bay is important for the heat transfer, and the global thermal efficiency η, defined below, is a major measure of the efficiency of the system:

$$\eta = (T_{\text{inlet}} - T_{\text{exhaust}})/(T_{\text{inlet}} - T_{\text{external}})$$

where T_{inlet} represents the temperature inside the piccolo tube, T_{exhaust} is the temperature at bay exhaust holes, and T_{external} is the temperature at the flight altitude.

A 3-D bay model is defined as one span segment of the wing leading edge anti-icing bay (**Figure 1**). It consists of the following: (1) a piccolo tube with a number of small holes to let the hot air impinge onto the leading edge. The small holes are in two rows in angles of 15° upper and lower from the wing chord plane; (2) the leading edge skin to be heated by the hot air in the anti-icing operation; (3) the exhaust holes on the lower side of the bay to allow the hot air to exit to the exterior flow; (4) two ribs (side walls) to separate the bays, with the hoses on the ribs neglected; and (5) the heat shield serving as the back wall of the bay model. The diameter of the piccolo tube remains constant even though the bay itself is slightly tapered.

2.2. The Numerical Approach

The CFD analysis tool used in this research is a well-known commercial Navier-Stokes solver Fluent V6.0 (Fluent V6.0, 2002). Its reliability has been demonstrated by a large number of aerospace and industrial applications.

An unstructured grid is used because of the complexity of the 3-D configuration. There are 281 980 nodes in the 3-D mesh and 21 330 nodes in the 2-D slice grid. Mesh adaption based on turbulent intensity is tested in 2-D simulations, but the results are found to be quite similar, as the original mesh is already fine enough. In the integrated interior–exterior thermal flow analysis, structured mesh is used. Details will be given later.

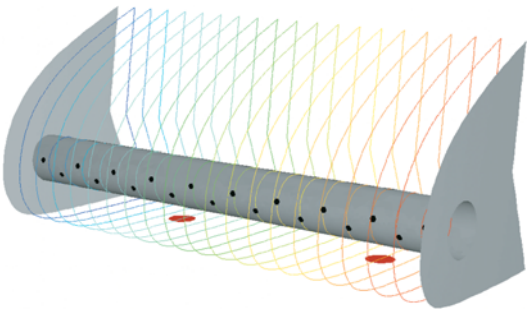

Figure 1. Three-dimensaionl bay model with two exhaust holes (the skin and heat shield shown by wires).

One- and two-equation turbulent models are tested for the viscous flow simulation, and the RNG k-ϵ Model, based on the renormalization group method, is selected because of its strength in simulating highly curved flows and wall heat transfers. Because the flow becomes compressible, the second-order upwind schemes are used in both 2-D and 3-D calculations.

Pressure inlet and outlet conditions are used at the piccolo tube holes and the exhaust holes. The turbulent specification methods at the inlet boundary are the intensity and the hydraulic diameter, reflecting the size of the small holes. For the bay internal flow simulation, the inlet and outlet conditions are selected based on the flight test measurements (Bombardier Aerospace, 2002).[1] For example, one inlet condition is P = 90 000 Pa, T = 453 K in the Piccolo tube, while the outlet condition is P = 63 000 Pa and T = 343 K at the exhaust holes of the bay.

2.3. The Numerical Results

Figure 2 shows the velocity vectors colored by the velocity magnitude (m/s), injecting from the piccolo tube holes, flowing over the inner skin and the piccolo tube surfaces and draining through the exhaust holes.

Figure 3 plots part of the streamlines inside the bay. The flow in the lower part of the bay is mainly chord-wise and has higher speed. Mixed 3-D flow could be seen in the upper part of the bay, and clear cross flow exists near the upper-rear corner of the bay. However, because of the very small magnitude of the cross flow velocity, it may not significantly affect the values of the flow characteristics, such as the pressure and the temperature in the span direction there.

Flow characteristics are examined to investigate the inference of the 3-D effects. **Figure 4** shows the skin friction coefficient C_f distributions. It is observed that the skin friction in the front leading edge is strong. The lower surface transfer is

[1] Please note that all flight test data presented in this paper are representative only to an actual airplane with a similar anti-icing system, exact design configurations are not provided. The bay model in this paper is generated according to the plots of the system so the geometry data may not necessarily be exact.

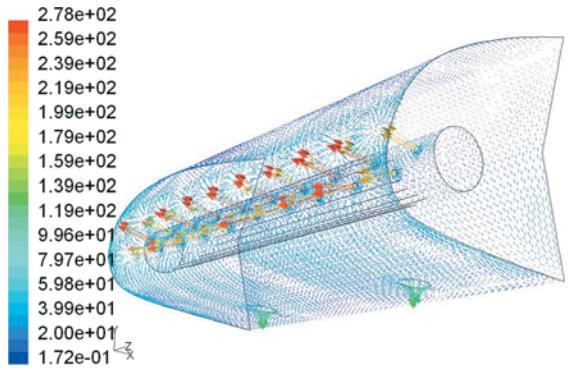

Figure 2. Velocity vectors (m/s).

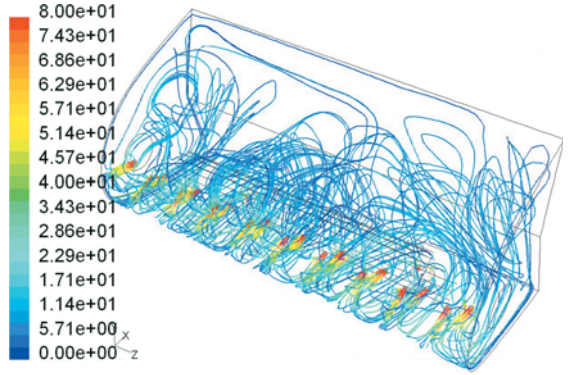

Figure 3. Part of the streamlines inside the bay (colored by velocity magnitude (m/s)).

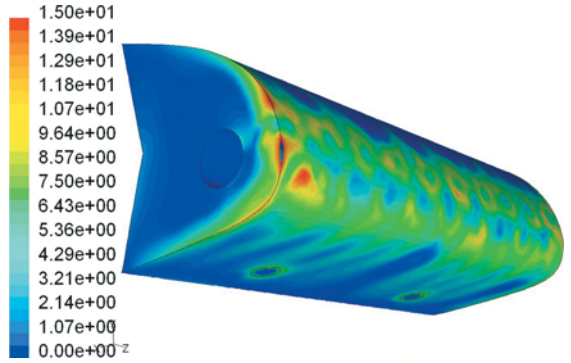

Figure 4. Skin friction coefficient distributions of the inner surface of the 3-D bay.

chord-wise dominant. And the upper surface exchange is weak but roughly uniform.

2.4. Comparison of the Two- and Three-Dimensional Flow Fields

To evaluate the slice approximation assumption, 2-D slices are computed separately and compared with the flow fields of a couple of span sections of the 3-D bay, for example, the cross sections with and without injection holes, and those with and without exhaust holes. In the 2-D slice model, the injection and exhaust holes are modified into slots, the width of which is chosen to match the total injection and exhaust areas of the 3-D bay.

Flow parameters, such as velocity V(m/s), Mach number M, the respective total and static pressures P_0 and P (Pa), the total and static temperatures T_0 and T (K), the skin friction coefficient C_f from both 2-D and 3-D computations, are also examined and compared, to further investigate the slice approximation.

The streamlines of a 3-D section are compared with those of a 2-D slice in **Figure 5**. Both sections have a lower 15° injection, with the exception that an exhaust slot exists in the 2-D model. The injecting flow between the piccolo tube and the leading edge could be seen in both 2-D and 3-D sections. The large vortex in the lower part of the bay behind the piccolo tube exists in both sections. The other large vortex in the upper rear part of the 2-D field does not appear clearly in the 3-D section because of the dominant mixed and cross flow.

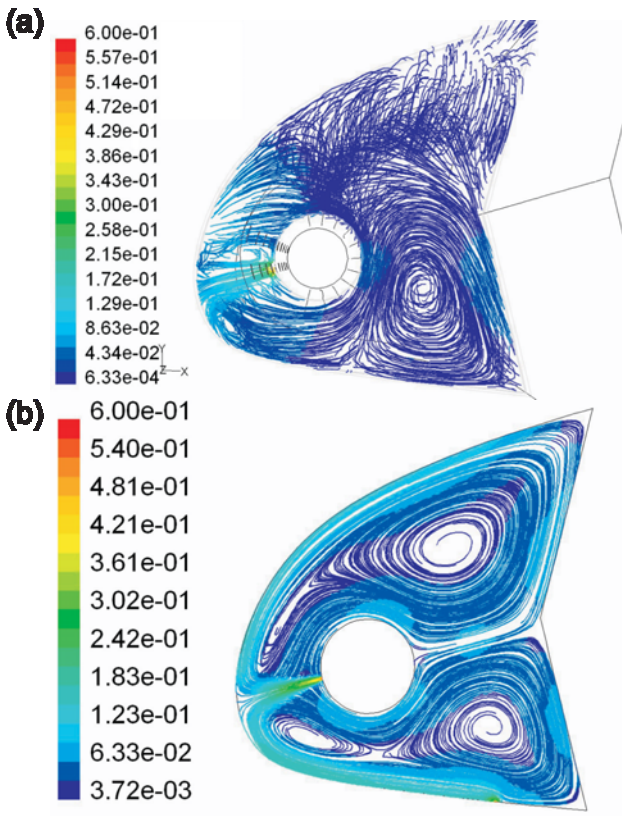

Figure 5. Comparison of flow fields colored by Mach number: (a) one cross section in 3-D bay; (b) corresponding 2-D slice.

However, the 3-D skin friction coefficient C_f appears as low as only approximately 1/2 to 1/3 the values of the corresponding 2-D computations for the lower surface and only 1/10 the values for the upper surface. The only exception is located at the leading edge area where the hot air impinges the internal skin surface, where the 2-D and 3-D values are close. The reason of this 2-D to 3-D discrepancy lies in the difference of the local flow speed, as discussed before. The 2-D flow

speed near the inner upper surface is higher than the 3-D values. This phenomenon suggests that the heat transfer might be over-estimated in 2-D results, particularly at the upper surface. Therefore, special attention should be given when one chooses the 2-D approximation model. Data tuning, correction, and validation are necessary when estimating the 3-D bay flows using the 2-D results.

3. Flow and Thermal Analysis of the Integrated Interior–Exterior Flows

3.1. Integrated Interior–Exterior Model

To calculate the exterior skin temperature of the wing leading edge, the thermodynamic analysis is applied to a geometry model that is constructed to include both internal and external flows. For the purpose of accurate external flow simulations, the complete wing, or at least a complete wing section, must be taken into account. In this paper, we present an example of such a simulation in two dimensions. A supercritical wing section NPU-SP8 (Hua and Zhang, 1990) is selected and modified so that the leading edge is more close to the above bay model. The aforementioned 2-D bay model is then inserted into the first 7% of the airfoil. It has 1.263 m chord length. The leading edge skin is modeled as a 1.7-mm-thick aluminum sheet. The viscous heat transfer between the skin and the interior–exterior fluid flows and the heat conductivity inside the aluminum skin are included in the simulation. The exterior flow is initiated from a pressure far-field boundary condition. The hot air injection is set up as a pressure inlet condition in the piccolo tube. The interior hot flow and the exterior dry-air flow fields are connected through the exhaust slot in the lower side of the bay. The widths of the injecting and exhaust slots in the 2-D models are chosen to match the total injection and exhaust areas of the 3-D bay.

To achieve more accurate simulations of the viscous effect and heat transfer with limited number of grid cells, the structured mesh is generated for both interior and exterior flow fields, as well as inside the solid skin, as partly shown in **Figure 6**. Boundary layer mesh of 20 layers is used over all the wing surfaces, and the grids are refined near the injection and impinging area. There are only 28 575 cells used in the 2-D grid, taking advantage of the structured mesh.

3.2. Interior–Exterior Thermal Flow Analysis

The far-field flow conditions are defined as follows: Mach number is 0.28, angle of attack is 4.5°, static pressure is 63 000 Pa, and static temperature is 263 K. The hot air inlet condition is chosen the same as in the 3-D bay cases. The pressure outlet condition at the exhaust is not required for this configuration. The CFD simulation presented in this paper is valid only for a dry-air flight. Super-cooled droplet impingement, evaporation, and the icing process are not treated.

A typical integrated interior–exterior thermodynamic analysis result is shown in **Figure 7**, plotted as Mach contours.

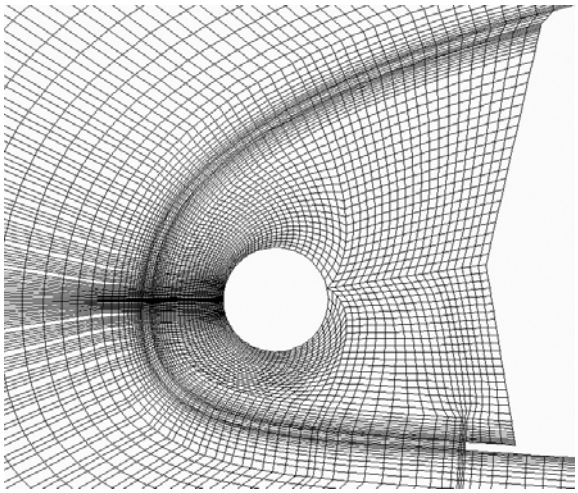

Figure 6. Part of the structured mesh.

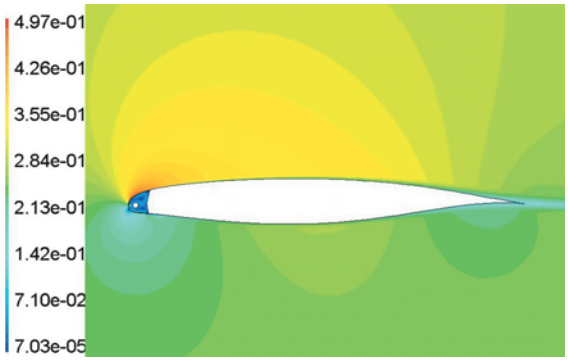

Figure 7. Mach contours of the interior–exterior flows.

It shows that, compared with the exterior flow, the interior flow is very slow.

Three injection slots are located at the front side of the piccolo tube. Two are located at 15° upper and lower positions from the chord direction, respectively, and the third one is set in between, on the chord plane. By specifying either pressure inlet boundary conditions or wall boundary conditions, the injection holes can be activated separately.

Figure 8a shows the static temperature contour of a single injection slot case denoted by "1-jet-chord". The injection is on the chord direction. The temperature distributions inside the aluminum skin and in both the internal and external flow fields are well illustrated. The temperature boundary layers can be clearly observed in an enlarged part, as shown in **Figure 8b**.

The skin temperature decreases towards the upper-rear corner of the bay, as discussed in Sect. 2. The higher local speed of the external flow brings away a lot of heat, and the slow interior flow cannot supply enough heat. As an attempt to increase the temperature near the upper-rear corner, another injection simulation is carried out with the slot located 15° up position to the chord direction, denoted by "1-jet-15°-up". The temperature over the entire upper skin increases

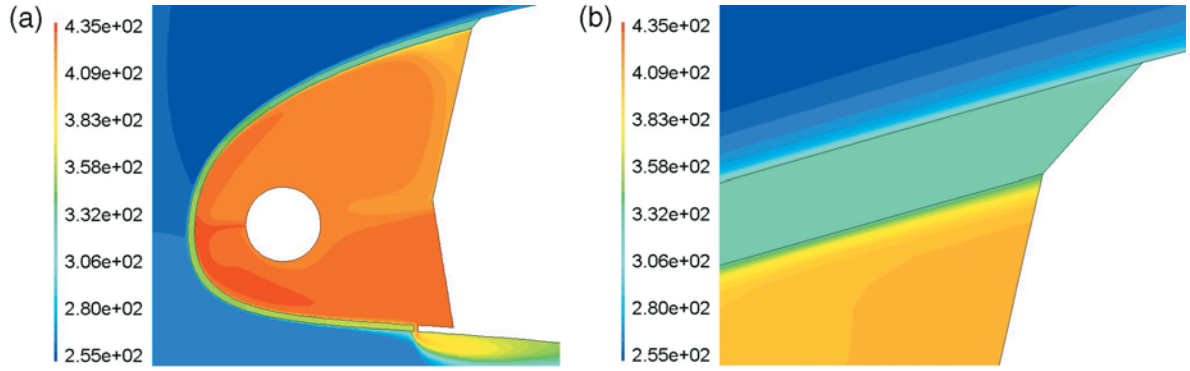

Figure 8. (a) Temperature distributions (K); (b) temperature boundary layers near the upper-rear corner of the bay (K).

correspondingly, and the temperature of lower surface decreases, as shown in **Figure 9**.

3.3. Comparison with Test Data

The 2-D internal–external coupled CFD results are compared with the available flight test data of an aircraft that has similar anti-icing configuration (Bombardier Aerospace, 2002).

The comparison is again for the dry air flight case only. The CFD boundary conditions are set to $M = 0.31$, angle of attack = 3.5°, P = 63 000 Pa, and T = 263 K for external flow; T_0 = 454 K and P_0 = 87 500 Pa for the internal flow at the piccolo tube holes.

Because of the difference in geometry details, and because the exact x coordinates of the temperature sensors are not specified (it is known only that the sensors in the flight test are located at the leading edge, the upper-rear-end, and the lower-rear-end of the bay), the comparison is then limited to the temperature region only, as shown in **Figure 10**.

The CFD estimated temperature is very close to the measurement at the leading edge. The upper surface values are overestimated, as we experienced before. The reason for the overestimation of the lower side is the exhaust slot in the 2-D model. The exhaust hot air greatly slows down the lower side flow between the stagnation point and the exhaust slot, leading to less external heat transfer there. The existence of the exhaust slot in the 2-D model also accelerates the internal flow along the lower side, causing more internal heat transfer.

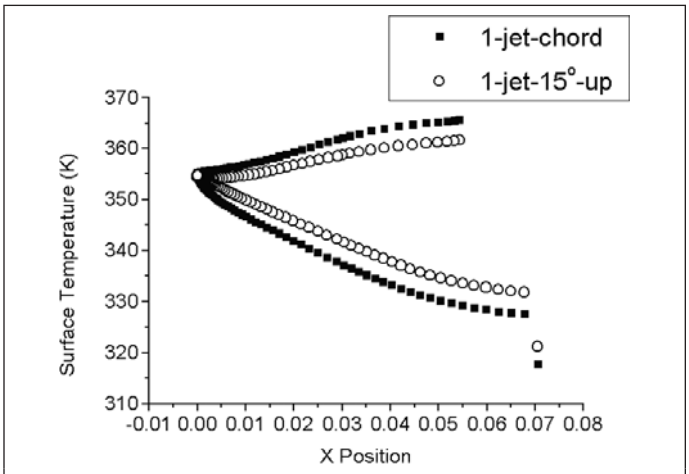

Figure 9. Temperature distributions over the outside surface of the bay for different slots orientations.

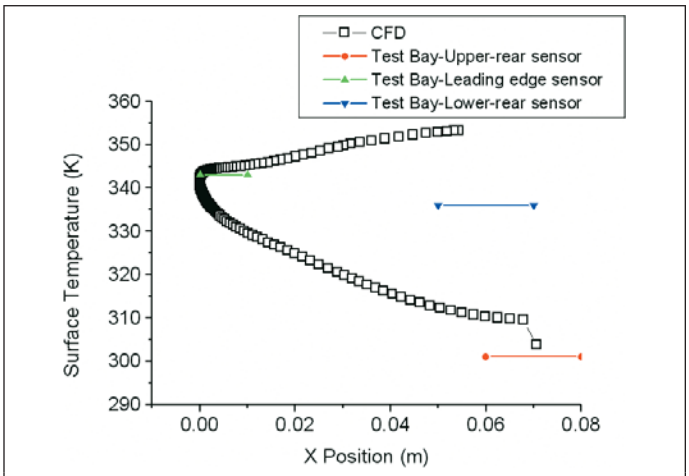

Figure 10. Temperature distributions over the outside surface of the bay and compared with test data.

4. Conclusions

The 3-D bay flow could be approximately simulated by the corresponding 2-D slice model from the perspective of the flow pattern. Most of the estimated 2-D flow characteristics are within 15% accuracy compared with their 3-D results, except for the surface friction coefficient. The comparisons suggest that the 2-D results may overestimate the internal heat exchange. The data correction and tuning are necessary in practice.

The integrated interior–exterior flow analysis of a complete wing section with the inserted leading edge anti-icing bay is conducted. It takes the real skin heat transfer and conductivity into account, so as to obtain the temperature distributions over the skin surface of the bay under actual dry air flight conditions.

The surface temperature distributions could be modified for given inlet and far field conditions by adjusting the hot air injection directions.

The surface temperature estimated from the 2-D CFD simulation is observed to be within the test data region. However, the upper and lower surface temperature values tend to be overestimated. Future work will include the 3-D integrated interior–exterior thermodynamic analysis of a reasonable wing–bay anti-icing system model and unsteady CFD investigations.

Acknowledgements

The research project is supported by the Ontario Research & Development Challenge Fund (ORDCF), and the Research Grant of the Natural Science and Engineering Council of Canada (NSERC). It is also in collaboration with Bombardier Aerospace. The authors would like to thank Professor David Zingg of UTIAS and anonymous reviewers for their comments and constructive suggestions.

References

Bombardier Aerospace. (2002). "Wing anti-icing flight test data".

Bourgault, Y., Boutanios, Z., and Habashi, W.G. (2000). "Three-dimensional Eulerian Approach to Droplet Impingement Simulation Using FENSAP-ICE, Part1: Model, Algorithm, and Validation". *J. Aircr.* Vol. 37, No. 1, pp. 95–103.

Beaugendre, H., Morency, F., and Habashi, W.G. (2003). "FENSAP-ICE's Three-Dimensional In Flight Ice Accretion Module: ICE3D". *J. Aircr.* Vol. 40, No. 2, pp. 239–247.

de Mattos, B.S., and Oliveira, G.L. (2000). "Three-dimensional Thermal Coupled Analysis of a Wing Slice Slat with a Piccolo Tube". *Proceedings of the AIAA Applied Aerodynamics 18th Conference*, Denver, Colorado. 14-17 August 2000. AIAA-2000-3921.

Fluent V6.0. Available from http://www.fluent.com [accessed 2002].

Frick, C.W., Jr., and McCullough, G.B. (1942). "A Method for Determining the Rate of Heat Transfer from a Wing or Streamline Body". NACA Report 830.

Hua, J., and Zhang, Z.Y. (1990). "Transonic Wing Design for Transport Aircraft". ICAS-90–3.7.4.

Morency, F., Tezok, F., and Paraschivoiu, I. (1999). "Anti-Icing System Simulation Using CANICE". *J. Aircr.* Vol. 36, No. 6, pp. 999–1006,

Wang, D., Naterer, G.F., and Wang, G. (2003). "Thermofluid Optimization of a Heated Helicopter Engine Cooling-Bay Surface". *Can. Aeronaut. Space J.* Vol. 49, No. 2, pp. 73–86.

